Journal of Solid State Chemistry **149,** 33–40 (2000)
Article ID jssc.1999.8490, available online at http://www.idealibrary.com on IDEAL®

Phase Stability of the System Mg–Fe–O

Sun-Ho Kang, Se-Hong Chang,[1] and Han-Ill Yoo[2]

Solid State Ionics Research Laboratory, School of Materials Science and Engineering, Seoul National University, Seoul 151-742, Korea

Received April 28, 1999; in revised form August 13, 1999; accepted August 27, 1999

The electrical conductivity and thermoelectric power of the system Mg–Fe–O were measured as functions of oxygen activity (a_{O_2}) and cationic composition in the temperature range $1100 \leq T/°C \leq 1300$. The isotherms of both electrical properties underwent a conspicuous change in trend at the same, characteristic oxygen activities, which was ascribed to a_{O_2}-induced phase transitions from rock-salt structure to spinel structure to corrundum structure with successively increasing a_{O_2}'s. The region of thermodynamic stability of each phase could be determined from either of the isotherms to construct phase diagrams of the first kind (i.e., log a_{O_2} vs $1/T$) for fixed compositions and the second kind (i.e., log a_{O_2} vs composition) at fixed temperatures. From the phase diagrams of the first kind, thermodynamic quantities for a phase boundary reaction, $4Fe_3O_4 + O_2(g) = 6Fe_2O_3$, were extracted and compared with those for other systems of ferrite. © 2000 Academic Press

***Key Words*: Mg ferrite; phase stability; phase diagrams; electrical conductivity; thermoelectric power.**

I. INTRODUCTION

A Me–Fe–O system (Me = Mg, Mn, Ni, Zn, etc.) has more than one crystallographic structure, depending on oxygen activity, a_{O_2} ($= P_{O_2}$/atm), at a given temperature and cationic composition, e.g., rock-salt structure phase, $(Me,Fe)_{1-\eta}O$, spinel structure phase, $(Me,Fe)_{3-\delta}O_4$, and corrundum structure phase, $(Me,Fe)_{2-\varepsilon}O_3$ (1–3). In preparation of spinel ferrite, $(Me_xFe_{1-x})_{3-\delta}O_4$, therefore, a precise control of oxygen activity during sintering and the cooling process is crucial to avoid undesirable precipitation of second phases which generally deteriorate the electrical and magnetic properties of the ferrite. Thus, for the purpose of tailoring high-quality ferrite, the exact stability region of the spinel phase at elevated temperatures must first be determined (4–6).

In this work, the phase stability of the system Mg–Fe–O was investigated *in situ* on the basis of electrical property–phase stability correlation. For this purpose, the electrical conductivity (σ) and thermoelectric power (θ) of the system were measured as functions of oxygen activity (a_{O_2}) and cationic composition [$x \equiv N_{Mg}/(N_{Mg} + N_{Fe})$, N_k being mole number of k] in thermodynamic equilibrium at elevated temperatures.

The electrical property–phase stability correlation has often been utilized to locate phase boundaries of spinel ferrite systems since Tannhauser (7) measured the electrical conductivity and thermoelectric power of the binary system Fe–O (wüstite, magnetite, and hematite) as a function of oxygen activity at elevated temperatures in 1962. He reported that those electrical properties changed discontinuously at the phase boundaries that had earlier been determined by Darken and Gurry (8). Vogler (9) and Tsuji *et al.* (10) later extended the idea of electrical property–phase stability correlation to multicomponent spinel ferrite systems such as MnZn ferrites and Mn ferrites, respectively, to determine their phase stability regions. Their studies, nevertheless, were confined to high oxygen activity regions and, hence, only the upper boundary of the single-phase field of spinel ferrite, i.e., the ferrite/hematite boundary, could be determined.

The most extensive and systematic studies on the phase stability of spinel ferrite systems using the electrical property–phase stability correlation were carried out by Yoo *et al.* (1, 2, 11–14). They measured electrical conductivity and thermoelectric power on various spinel ferrites (Mn, Zn, and MnZn ferrites) at elevated temperatures over an extensive range of oxygen activity and constructed the phase stability diagrams on the plane of log a_{O_2} vs temperature, i.e., phase diagrams of type I. Through a number of studies, they demonstrated that the electrical properties can be utilized as a simple, economic means to determine *in situ* the stability fields of spinel ferrites.

This article reports two types of phase stability diagrams for the system Mg–Fe–O: phase diagrams of type I (a_{O_2} vs T) for fixed cationic compositions and phase diagrams of type II (a_{O_2} vs x) at fixed temperatures on the basis of the well-established electrical property–phase stability correlation. Furthermore, thermodynamic quantities for a phase

[1] Present address: Korea Electronics Technology Institute, #455-6 MaSan-Ri, JinWi-Myon, Pyung Taek-Gun, KyungGi-Do 451-860, Korea.
[2] To whom correspondence should be addressed. E-mail: hiyoo@plaza.snu.ac.kr.

0022-4596/00 $35.00

boundary reaction, $4Fe_3O_4 + O_2(g) = 6Fe_2O_3$, were evaluated from the phase diagrams of the first kind and compared with those of other ferrite systems.

II. EXPERIMENTAL

Polycrystalline ferrite specimens, $(Mg_xFe_{1-x})_{3-\delta}O_4$, of three different cationic compositions (x) were prepared from the starting powders of α-Fe_2O_3 (99.99%, High Purity Chemicals Co., Japan) and MgO (99.99%, Yamanaka Chemical Industries Ltd., Japan) via a conventional ceramic processing route. Sintering was carried out at 1350°C in air for about 2 h. The cationic compositions of the specimens were subsequently assayed as $x = 0.295$, 0.247, and 0.169 by ICP-emission spectrophotometry, the error bounds of which were about $\pm$ 0.007.

The electrical conductivity (σ) and thermoelectric power (θ) of the three samples were measured by a dc four-probe technique and a heat pulse technique (11–13), respectively, as functions of oxygen activity (a_{O_2}) in the temperature range $1100 \leq T/°C \leq 1300$. For the electrical property measurements, the sintered ferrite disks were cut into parallelepipeds measuring ca. 2 mm × 2 mm × 18 mm, and two pieces of Pt wire, as voltage probes in the conductivity measurement, were attached at about 3.5 mm from each end of a parallelepiped. For the measurements of temperature and thermoelectric power, a thermocouple of type S (Pt–Pt10Rh) with a flattened bead was made in contact with each end face of the parallelepiped by applying a light spring pressure. The Pt legs of these two thermocouples were also used as the current probes for the conductivity measurement. A small resistance heater, a platinum wire of 0.18 mm diameter embedded in an alumina plate, was placed at one end of the specimen to generate a heat flux (11). The experimental setup is schematically illustrated in Fig. 1.

The ambient oxygen activity was controlled by using N_2/O_2 or CO_2/CO gas mixtures and monitored with an oxygen concentration cell based on stabilized zirconia (11). Current was applied with the use of a constant-current supplier (Keithley, 224 programmable current source) and all signals, including temperature and voltage drop, were measured with a digital multimeter (Keithley, DM 196 system).

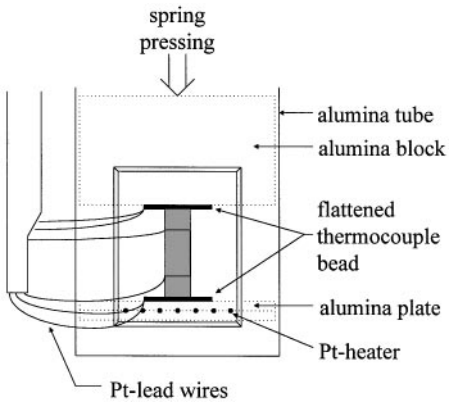

FIG. 1. Schematic diagram of electrical conductivity and thermoelectric power measuring unit.

III. RESULTS AND DISCUSSION

III.1. Electrical Properties and Phase Stability of the System Mg–Fe–O

The isothermal variations of electrical conductivity (σ) and thermoelectric power (θ) against a_{O_2} for different compositions (x) at 1100, 1200, and 1300°C are shown in Figs. 2a, 2b, and 2c, respectively.

In calculating the electrical conductivity from a measured conductance, the geometric factor of a specimen (the cross-sectional area divided by the distance between the voltage probes) that was previously measured on the as-prepared specimen (of spinel phase) at room temperature was used, and the dimensional variation due to temperature and phase changes of the specimen was not taken into account. This simplification may cause an error in the electrical conductivity values, but it should not affect the phase boundaries therefrom because those are determined from the relative variation of conductivity against oxygen activity. The as-measured thermoelectric power was corrected against the absolute thermoelectric power of Pt (15) to obtain the absolute thermopower of the specimen.

According to the Gibbs phase rule, the number of independent variables of the system Mg–Fe–O is 2 in single-phase regions and 1 in two-phase regions at a fixed temperature and total pressure. Furthermore, in single-phase regions, e.g., $(Mg_xFe_{1-x})_{1-\eta}O$ and $(Mg_xFe_{1-x})_{3-\delta}O_4$, the metallic components are little volatile so that the Mg/Fe molar ratio may remain unchanged across the single-phase regions. This constraint further reduces the degrees of freedom of the system to 1 in the single-phase regions. Consequently, both in the single-phase regions and in the two-phase regions, the number of independent thermodynamic variables is 1, and the oxygen activity (a_{O_2}) can thus be chosen as the single independent variable at a given temperature. This explains the uniqueness of the isotherms in Figs. 2a–c as has been confirmed repeatedly (2, 11–14, 16).

One can see in Figs. 2a–c that all of the conductivity isotherms exhibit the same features regardless of compositions and temperatures: as a_{O_2} decreases from 1, the conductivity first increases and then shows a negligible dependence on a_{O_2}. As a_{O_2} decreases further, the conductivity increases again, leaving a maximum, decreases monotonically, and finally increases sharply at a very low oxygen activity. At the same characteristic oxygen activities as those on the conductivity isotherms, the thermopower isotherms also undergo conspicuous changes.

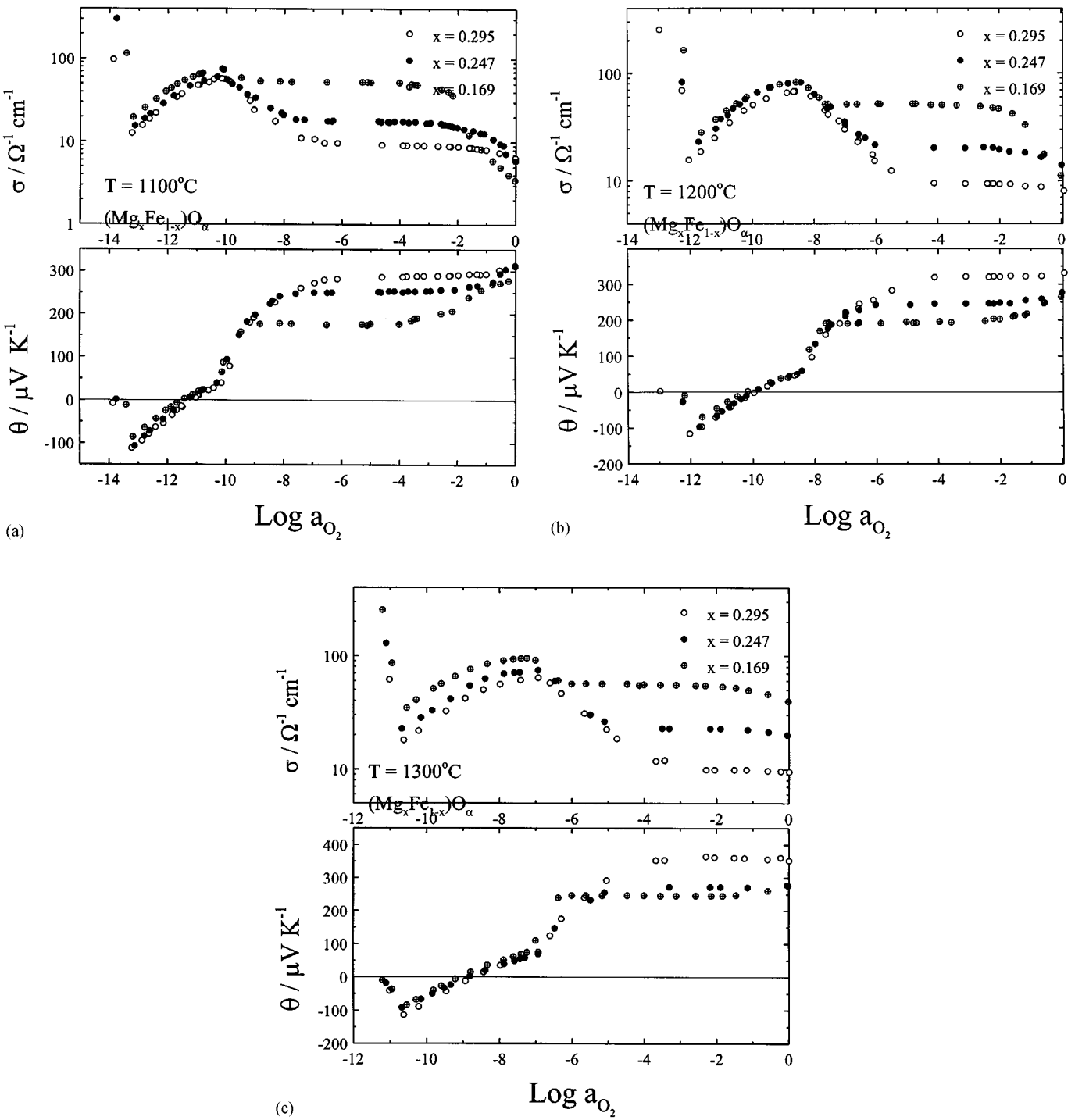

FIG. 2. Electrical conductivity (upper) and thermoelectric power (lower) isotherms measured at (a) 1100, (b) 1200, and (c) 1300°C as a function of oxygen activity.

To show these trends more clearly, the two isotherms for the composition $x = 0.169$ at 1200°C are reproduced in Fig. 3. On these isotherms, five oxygen activity regions may be distinguished, which are denoted by Roman numerals I to V. Each regime is bounded by the onsets of transition of both electrical properties, i.e., conductivity minimum, conductivity maximum, and points where the conductivity begins to increase or decrease. The same is true for the corresponding thermopower isotherm. As is seen, an exact one-to-one correspondence exists between the

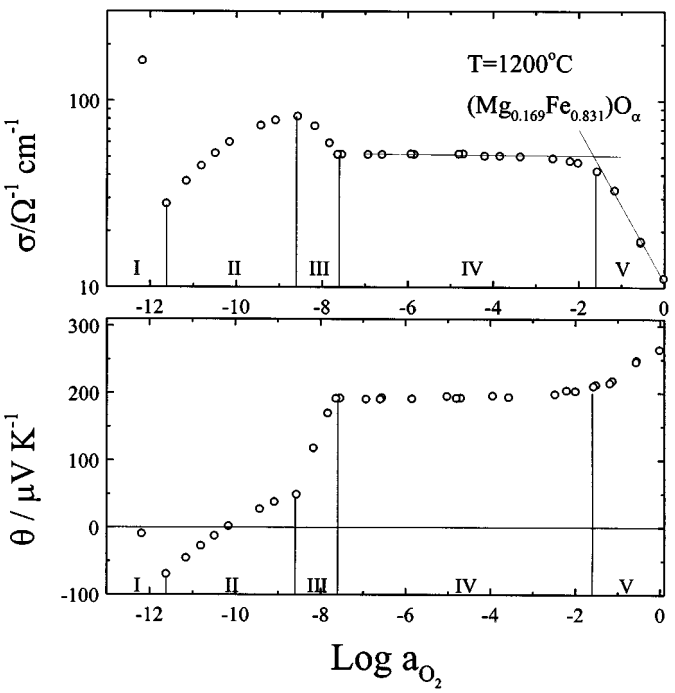

FIG. 3. Electrical conductivity (upper) and thermoelectric power (lower) isotherms of $(Mg_{0.169}Fe_{0.831})O_\alpha$ measured at 1200°C as a function of oxygen activity. I, Fe + $(Mg,Fe)_{1-\eta}O$; II, Fe + $(Mg,Fe)_{1-\eta}O$; III, $(Mg,Fe)_{1-\eta}O$ + $(Mg,Fe)_{3-\delta}O_4$; IV, $(Mg,Fe)_{3-\delta}O_4$; V, $(Mg,Fe)_{3-\delta}O_4$ + Fe_2O_3

characteristic points on the conductivity and thermopower isotherms.

Yoo *et al.* (1, 2, 11–14) have reported similar features on various spinel ferrites and confirmed that those conspicuous changes in conductivity and thermopower are due to phase transitions at the corresponding oxygen activities. On the basis of this electrical property–phase stability correlation, the five different regions in Fig. 3 can be assigned as follows: (I) a two-phase region of Fe metal and rock-salt structure $(Mg,Fe)_{1-\eta}O$ (designated MW); (II) a single-phase region of rock-salt structure $(Mg,Fe)_{1-\eta}O$; (III) a two-phase region of rock-salt structure and spinel structure $(Mg,Fe)_{3-\delta}O_4$ (designated MF); (IV) a single-phase region of spinel structure $(Mg,Fe)_{3-\delta}O_4$; and (V) a two-phase region of spinel structure and corrundum structure Fe_2O_3 (designated H). In this manner, all of the isotherms in Figs. 2a–c were analyzed, and the phase boundaries determined thereby for each cationic composition and temperature are listed in Table 1. The validity of the demarcation of each phase field as in Fig. 3 is well established in the literature (2, 3, 12, 16). Only the way of determination of the single-phase region of the spinel ferrite will be discussed below.

The electrical conductivity of spinel ferrites, $(Me_xFe_{1-x})_{3-\delta}O_4$, with excess iron (i.e., $x < 1/3$) has been reported to be essentially independent of a_{O_2} (1–3, 11–14, 16), as is found in the present work. This is attributed to the fact that the concentration of electronic charge carriers is governed primarily by molecularity, or the cationic composition, rather than by oxygen nonstoichiometry (11, 12). In this respect, the decrease in conductivity found at higher oxygen activity (in region V in Fig. 3) may be regarded as being due to precipitation of a more resistive phase, e.g., hematite. The point where the conductivity starts to decrease, however, cannot be assigned unambiguously to the upper boundary of the spinel field because the nonstoichiometry or metal deficit (δ) also increases appreciably as the upper boundary is approached. In magnetite, $Fe_{3-\delta}O_4$, for example, the extent of the nonstoichiometry (δ) at the magnetite/hematite boundary amounts to $\delta \approx 0.05$ at 1200°C (17), and this large nonstoichiometry causes the electrical conductivity of magnetite to decrease by about 10% near the upper boundary of the magnetite bordering the hematite phase (18). Although the magnitude of the maximum nonstoichiometry tends to reduce with increasing Mg content (x) (19, 20), the effect of nonstoichiometry on the electrical conductivity near the upper boundary must also be taken into account. In this work, thus, the point where the two tangential lines intersect as depicted in Fig. 3 is assigned as the upper boundary of the spinel ferrite as was practiced by Subramanian *et al.* (3) in determining the upper boundary of $(Co, Fe, Mn)_{3-\delta}O_4$. The uncertainty of the boundary determined in this way is believed to be no greater than ± 0.5 in log a_{O_2} on the basis of experience (2, 3, 12, 16). It appears that for the compositions of $x = 0.295$ and 0.247 at 1300°C, the upper boundaries are not crossed up to $a_{O_2} = 1$.

The lower boundaries of the spinel phases were determined as the point where the electrical conductivities start to increase as shown in Fig. 3. According to Paladino (21), magnesio wüstite $(Mg, Fe)_{1-\eta}O$, which precipitates out of

TABLE 1
Phase Boundaries of the System Mg–Fe–O Determined by Electrical Means

Composition, x	Phase boundary	1100°C	1200°C	1300°C
0.295	(H + MF)/MF	− 1.3[a]	− 0.7	—
	MF/(MF + MW)	− 6.7	− 4.8	− 3.8
	(MF + MW)/MW	− 10.2	− 8.5	− 6.8
	MW/(MW + Fe metal)	− 13.4	− 12.1	− 10.9
0.247	(H + MF)/MF	− 1.9	− 1.5	—
	MF/(MF + MW)	− 7.8	− 6.1	− 4.7
	(MF + MW)/MW	− 10.3	− 8.5	− 7.3
	MW/(MW + Fe metal)	− 13.4	− 12	− 10.8
0.169	(H + MF)/MF	− 2.4	− 1.6	—
	MF/(MF + MW)	− 9.2	− 7.6	− 6.2
	(MF + MW)/MW	− 10.4	− 8.6	− 7.1
	MW/(MW + Fe metal)	− 13.3	− 11.9	− 10.8

[a] Phase boundaries are expressed in log a_{O_2}. H, hematite; MF, magnesioferrite; MW, magnesiowüstite.

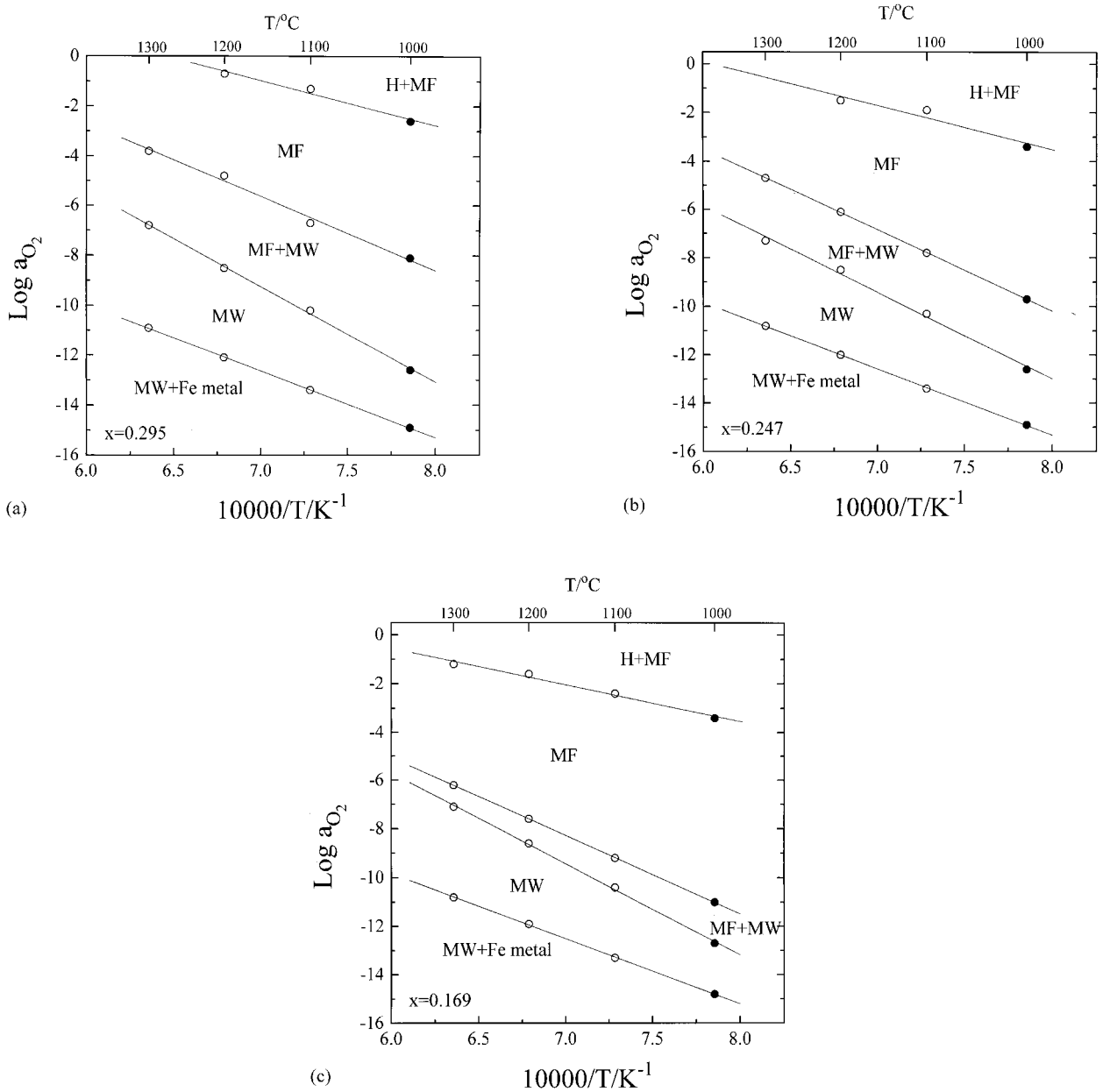

FIG. 4. Phase diagrams of type I for the Mg–Fe–O system: (a) $x = 0.295$, (b) $x = 0.247$, and (c) $x = 0.169$. The data at 1000°C (solid circles) are from Zalazinskii *et al.* (22). Solid lines are linear regression results. H, hematite; MF, magnesioferrite; MW magnesiowüsitite.

magnesio ferrite $(Mg, Fe)_{3-\delta}O_4$, consists largely of MgO. Since magnesio wüstite precipitates out of the spinel ferrite, therefore, the spinel ferrite in the two-phase mixture contains less Mg than the spinel single phase does. One can see in Figs. 2a–c that as Mg content decreases, the electrical conductivity of the spinel ferrite increases. Accordingly, the precipitation of magnesio wüstite induces an increase of Fe content in the matrix of the spinel phase, which causes the overall electrical conductivity to increase.

III.2. Construction of Phase Diagrams

With the phase boundaries determined above (Table 1), the phase diagrams of type I (a_{O_2} vs T) and type II (a_{O_2} vs composition) were constructed. All of the phase diagrams are illustrated in Figs. 4 and 5 together with the literature data (22).

One can see in Figs. 4a–c that all the phase boundaries show a good linearity over the temperature range 1000–

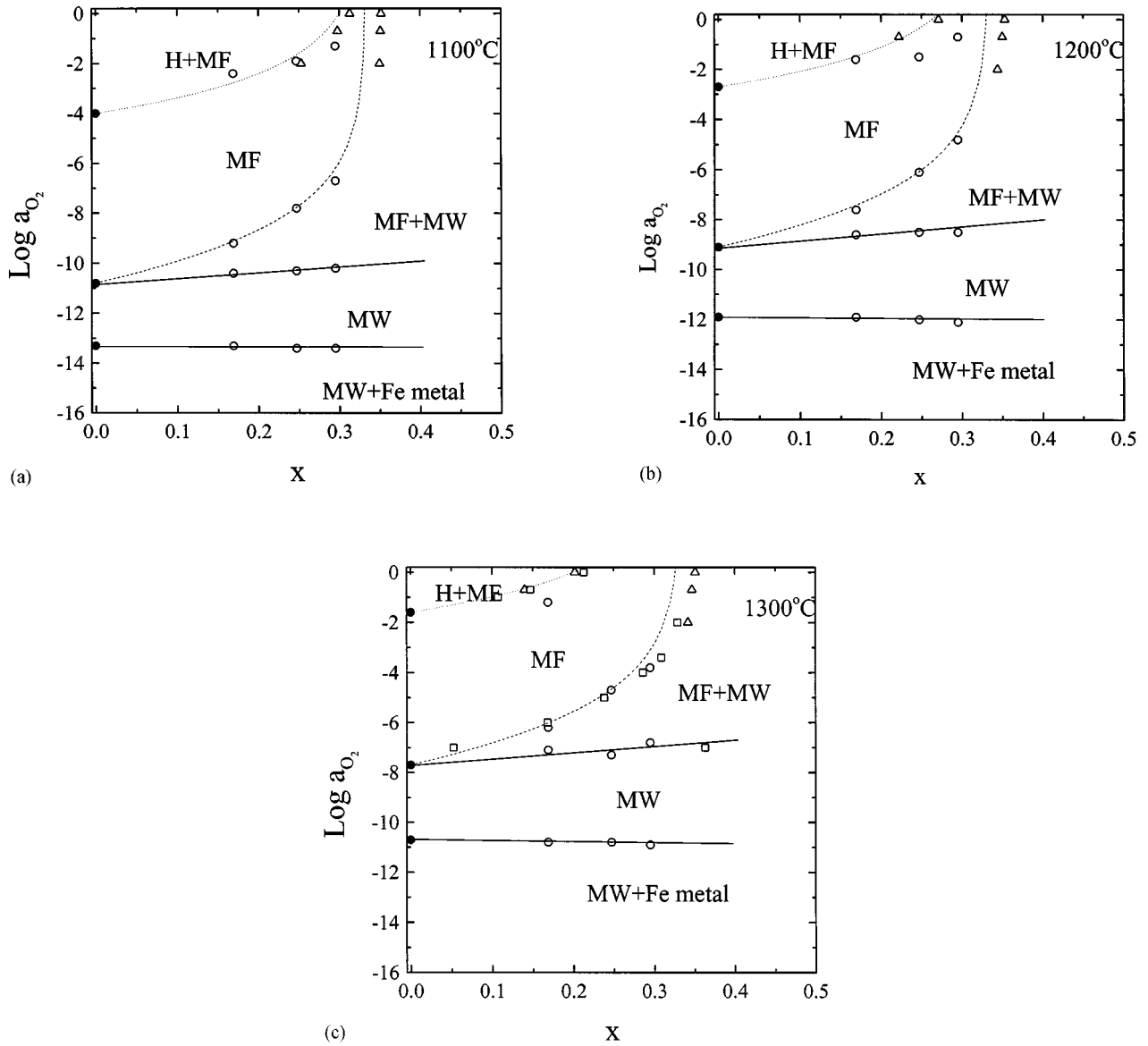

FIG. 5. Phase diagrams of type II for the Mg–Fe–O systems: (a) 1100, (b) 1200, and (c) 1300°C. The data for $x = 0$ are from the literature (24–26). Triangles and squares are from Paladino (21) and Speidel (23), respectively. Solid lines are for visual guidance. Dotted lines and dashed lines are calculated from Eqs. [4] and [5], respectively.

1300°C and they are well represented by a linear equation as depicted with solid lines,

$$\log a_{O_2} = A - B/T, \qquad [1]$$

where A and B are constants. The values of A and B for each phase boundary and composition obtained from linear regression are listed in Table 2.

At the phase boundary of MF/(MF + H), the following reaction may be considered to occur:

$$4\underline{Fe_3O_4}\ [\text{in } (Mg_xFe_{1-x})_{3\div\delta'}O_4] + O_2(g) = 6Fe_2O_3, \qquad [2]$$

where δ' is the upper limit of the nonstoichiometry of the spinel ferrite. Applying the mass action law with the assumption that the reaction equilibrium constant for the above reaction is independent of the composition (x), we obtain

$$K = \exp\left(-\frac{\Delta G^\circ_{sp/hem}}{RT}\right) = \frac{a^6_{Fe_2O_3}}{a^4_{Fe_3O_4}a_{O_2}} = \frac{a^{\circ 6}_{Fe_2O_3}}{a^{\circ 4}_{Fe_3O_4}a^\circ_{O_2}}, \qquad [3]$$

where K and $\Delta G^\circ_{sp/hem}$ are the reaction equilibrium constant and the standard free energy change, respectively, for the phase boundary reaction [2]. $a^\circ_{Fe_2O_3}$, $a^\circ_{Fe_3O_4}$, and $a^\circ_{O_2}$ are the

TABLE 2

Constants A and B in Eq. [1] for the Phase Boundaries in the Type I Phase Diagrams of the System Mg–Fe–O in the Temperature Range 1000–1300°C

Composition, x	Phase boundary[a]	A	B (K)
0.295	(H + MF)/MF	12 ± 2	$(1.8 \pm 0.3) \times 10^4$
	MF/(MF + MW)	15.1 ± 0.2	$(3.0 \pm 0.2) \times 10^4$
	(MF + MW)/MW	17.58 ± 0.12	$(3.8 \pm 0.1) \times 10^4$
	MW/(MW + Fe metal)	6.01 ± 0.03	$(2.7 \pm 0.3) \times 10^4$
0.247	(H + MF)/MF	11 ± 4	$(1.8 \pm 0.5) \times 10^4$
	MF/(MF + MW)	16.60 ± 0.03	$(3.35 \pm 0.02) \times 10^4$
	(MF + MW)/MW	15.5 ± 0.2	$(3.57 \pm 0.19) \times 10^4$
	MW/(MW + Fe metal)	6.63 ± 0.04	$(2.74 \pm 0.03) \times 10^4$
0.169	(H + MF)/MF	8.4 ± 0.9	$(1.49 \pm 0.13) \times 10^4$
	MF/(MF + MW)	14.17 ± 0.02	$(3.210 \pm 0.017) \times 10^4$
	(MF + MW)/MW	16.7 ± 0.1	$(3.74 \pm 0.09) \times 10^4$
	MW/(MW + Fe metal)	6.30 ± 0.04	$(2.69 \pm 0.04) \times 10^4$

[a] H, hematite; MF, magnesioferrite; MW, magnesiowüstite.

activities of Fe_2O_3, Fe_3O_4, and O_2, respectively, at the phase boundary of $Fe_{3-\delta}O_4/Fe_2O_3$ for the pure Fe–O system (i.e., $x = 0$). Because Fe_2O_3 is preferentially formed highly pure with negligible nonstoichiometry in the two-phase region of MF + H (23), $a_{Fe_2O_3}$ and $a^{\circ}_{Fe_2O_3}$ in Eq. [3] may be taken as unity. According to Schmalzried and Tretjakow (27), the activity of Fe_3O_4 at the phase boundary $Fe_{3-\delta}O_4/Fe_2O_3$, $a^{\circ}_{Fe_3O_4}$, may also be taken as 1 within an error range of less than 5%. Furthermore, with the assumption that $(Mg_xFe_{1-x})_{3-\delta}O_4$ is an ideal solution of Fe_3O_4 and $MgFe_2O_4$ (20), $a_{Fe_3O_4}$ can be set equal to $(1 - 3x)$. Therefore, it follows from Eq. [3] that

$$\log a_{O_2} = \log a^{\circ}_{O_2} - 4 \log(1 - 3x). \qquad [4]$$

The dotted lines in Figs. 5a–c are calculated from Eq. [4]. It is seen that the calculated curves agree reasonably well with the present and literature data. In practice, one may thus utilize Eq. [4] to predict the upper boundary of Mg ferrite with any composition.

As far as the phase boundary of (MW + MF)/MF is concerned, Schmalzried and Tretjakow (27) derived the following equation on the basis of defect chemistry:

$$\log a_{O_2} = \log a^{*}_{O_2} - 4 \log(1 - 3x) - 4 \log(1 - x) + 2 \log(1 + x), \qquad [5]$$

where $a^{*}_{O_2}$ is the activity of O_2 at the phase boundary of $Fe_{1-\Delta}O/Fe_{3-\delta}O_4$ for the pure Fe–O system. The dashed lines in Figs. 5a–c are calculated from Eq. [5]. At low Mg content (x), there exists quite good agreement between experimental and theoretical values. At Mg contents higher than about $x = 0.29$, however, a large discrepancy is found and the discrepancy becomes larger as Mg content increases. In the derivation of Eq. [5], Schmalzried and Tretjakow neglected the existence of interstitial Mg^{2+} for the sake of simplicity, and, consequently, the oxygen activity cannot be defined in Eq. [5] for the composition of $x > 1/3$. According to Paladino (21), the solubility limit of Mg in $(Mg_xFe_{1-x})_{3-\delta}O_4$ is $x = 0.352$ independent of temperature, and, therefore, $(Mg_xFe_{1-x})_{3-\delta}O_4$ ferrite can exist with excess Mg in the form of $(MgO)_yMgFe_2O_4$. Neglect of the existence of interstitial cations consequently caused the discrepancy at higher Mg contents as is seen in Fig. 5a–c.

III.3. Thermodynamic Calculation

If Eq. [4] were exact, then the standard free energy of reaction of Eq. [2] would be identical to that of the oxidation reaction of pure Fe_3O_4 to Fe_2O_3, or $4Fe_3O_4 + O_2 = 6Fe_2O_3$. It would immediately follow from Eq. [3] that

$$\ln a_{O_2} = -4 \ln(1 - 3x) - \frac{\Delta S^{\circ}_{sp/hem}}{R} + \frac{\Delta H^{\circ}_{sp/hem}}{RT}, \qquad [6]$$

where $\Delta S^{\circ}_{sp/hem}$ and $\Delta H^{\circ}_{sp/hem}$ are the standard entropy and enthalpy change, respectively, for the phase boundary reaction [2]. For the pure Fe–O system, $\Delta S^{\circ}_{sp/hem} \approx -280$ J/K and $\Delta H^{\circ}_{sp/hem} \approx -470$ kJ in the temperature range 1000–1300°C (28).

By comparison of Eqs. [1] and [6], $\Delta S^{\circ}_{sp/hem}$ and $\Delta H^{\circ}_{sp/hem}$ can be calculated as

$$\Delta S^{\circ}_{sp/hem} = -4R \ln(1 - 3x) - 2.303RA \qquad [7]$$

$$\Delta H^{\circ}_{sp/hem} = -2.303RB. \qquad [8]$$

$\Delta S^{\circ}_{sp/hem}$ and $\Delta H^{\circ}_{sp/hem}$ have thus been evaluated as $\Delta S^{\circ}_{sp/hem} = -160 \pm 40$ J/K · mol and $\Delta H^{\circ}_{sp/hem} = -350 \pm$

TABLE 3

Standard Enthalpy Changes for the Phase Boundary Reactions $4Fe_3O_4 + O_2(g) = 6Fe_2O_3$ in Various Ferrites

Ferrite	$\Delta H^{\circ}_{sp/hem}$ (kJ mol^{-1})	Reference
$Fe_{3-\delta}O_4$	−470	28
MnZn ferrites	−358	9
$Mn_{0.588}Zn_{0.333}Fe_{2.078}O_{4+\delta}$	-415 ± 3	29
$MnFe_2O_{4+\delta}$	-414 ± 13	10
$Mn_{0.953}Fe_{2.047}O_{4+\delta}$	-360 ± 20	2
$Mn_{0.54}Zn_{0.35}Fe_{2.11}O_4$	-287 ± 6	14
$(Mg_{0.295}Fe_{0.705})_{3-\delta}O_4$	-350 ± 60	Present work
$(Mg_{0.247}Fe_{0.753})_{3-\delta}O_4$	-300 ± 100	Present work
$(Mg_{0.169}Fe_{0.831})_{3-\delta}O_4$	-290 ± 30	Present work

60 kJ/mol for $x = 0.295$, $\Delta S^{\circ}_{sp/hem} = -170 \pm 80$ J/K · mol and $\Delta H^{\circ}_{sp/hem} = -300 \pm 100$ kJ/mol for $x = 0.247$, and $\Delta S^{\circ}_{sp/hem} = -140 \pm 20$ J/K · mol and $\Delta H^{\circ}_{sp/hem} = -290 \pm 30$ kJ/mol for $x = 0.169$. Literature data on $\Delta H^{\circ}_{sp/hem}$ in various ferrites are listed in Table 3 together with those of the present work for comparison.

IV. SUMMARY AND CONCLUSIONS

The phase stability of the system Mg–Fe–O was investigated via electrical conductivity and thermopower measurement. It was found that both of the electrical properties exhibited conspicuous changes at the same characteristic oxygen activities that were ascribed to phase boundaries. On the basis of this electrical property–phase stability correlation, the regions of thermodynamic stability of possible phases in the Mg–Fe–O system (Fe metal, rock salt, spinel, and corrundum structure phase) were determined to construct phase diagrams of the first kind (log a_{O_2} vs $1/T$) for fixed compositions and the second kind (log a_{O_2} vs composition) at fixed temperatures.

From the phase diagrams of the first kind, changes of enthalpy and entropy for the phase boundary reaction, $4\underline{Fe_3O_4}$ [in $(Mg_xFe_{1-x})_{3-\delta}O_4$] + $O_2(g) = 6Fe_2O_3$, were evaluated as $\Delta S^{\circ}_{sp/hem} = -160 \pm 40$ J/K · mol and $\Delta H^{\circ}_{sp/hem} = -350 \pm 60$ kJ/mol for $(Mg_{0.295}Fe_{0.705})O_{\alpha}$, $\Delta S^{\circ}_{sp/hem} = -170 \pm 80$ J/K · mol and $\Delta H^{\circ}_{sp/hem} = -300 \pm 100$ kJ/mol for $(Mg_{0.247}Fe_{0.753})O_{\alpha}$, and $\Delta S^{\circ}_{sp/hem} = -140 \pm 20$ J/K · mol and $\Delta H^{\circ}_{sp/hem} = -290 \pm 30$ kJ/mol for $(Mg_{0.169}Fe_{0.831})O_{\alpha}$.

REFERENCES

1. H. L. Tuller, H.-I. Yoo, W. Kehr, and R. W. Scheidecker, "Advances in Ceramics" (F. Y. Wang, Ed.), Vol. 15. Am. Ceram. Soc., Westerville, OH, 1985.
2. H.-I. Yoo and H. L. Tuller, *J. Mater. Res.* **3,** 552 (1988).
3. R. Subramanian and R. Dieckmann, *J. Am. Ceram. Soc.* **75,** 382 (1992).
4. T. G. Reynolds, III and R. C. Buchanan, *in* "Ceramic Materials for Electronics" (R. C. Buchanan, Ed.), Chap. 4. Dekker, New York, 1968.
5. P. I. Slick, *in* "Ferromagnetic Materials" (E. P. Wohlfarth, Ed.), Vol. 2, Chap. 3. North-Holland, New York, 1980.
6. J. Nicolas, *in* "Ferromagnetic Materials" (E. P. Wohlfarth, Ed.), Vol. 2, Chap. 4. North-Holland, New York, 1980.
7. D. S. Tannhauser, *J. Phys. Chem. Solids* **23,** 25 (1962).
8. L. S. Darken and R. W. Gurry, *J. Am. Chem. Soc.* **67,** 1398 (1945).
9. V. G. Vogler, *Z. Anorg. Allg. Chem.* **387,** 72 (1972).
10. T. Tsuji, W. Asakura, T. Yamashita, and K. Naito, *J. Solid State Chem.* **50,** 273 (1983).
11. H.-I. Yoo, and H. L. Tuller, *J. Am. Ceram. Soc.* **70,** 388 (1987).
12. J.-H. Kim, H.-I. Yoo, and H. L. Tuller, *J. Am. Ceram. Soc.* **73,** 258 (1990).
13. J.-H. Chae, H.-I. Yoo, S.-H. Kang, D.-S. Kang, and B.-D. You, *J. Kor. Ceram. Soc.* **32,** 394 (1995).
14. Y.-I. Jang and H.-I. Yoo, *Solid State Ionics* **84,** 77 (1996).
15. N. Cusack and P. Kendall, *Proc. Phys. Soc. London* **72,** 808 (1958).
16. J.-H. Chae, M.S. Thesis, Seoul National University, 1994.
17. R. Dieckmann, *Ber. Bunsenges. Phys. Chem.* **86,** 112 (1982).
18. R. Dieckmann, C. A. Witt, and T. O. Mason, *Ber. Bunsenges. Phys. Chem.* **87,** 495 (1983).
19. S.-H. Kang and H.-I. Yoo, *Solid State Ionics* **86–88,** 751 (1996).
20. S.-H. Kang and H.-I. Yoo, *J. Solid State Chem.* **139,** 128 (1998).
21. A. E. Paladino, *J. Am. Ceram. Soc.* **43,** 183 (1960).
22. A. G. Zalazinskii, V. F. Balakirev, V. P. Barkhatov, and G. I. Chufarov, *Russ. J. Phys. Chem.* (*Engl. Transl.*) **49,** 914 (1975).
23. D. H. Speidel, *J. Am. Ceram. Soc.* **50,** 243 (1967).
24. P. E. C. Bryant and W. W. Smeltzer, *J. Electrochem. Soc.* **116,** 1409 (1969).
25. R. A. Giddings and R. S. Gordon, *J. Am. Ceram. Soc.* **56,** 111 (1973).
26. H. F. Rizzo, R. S. Gordon, and I. B. Cutler, *J. Electrochem. Soc.* **116,** 266 (1969).
27. H. Schmalzried and J. D. Tretjakow, *Ber. Bunsenges. Phys. Chem.* **70,** 180 (1966).
28. I. Barin, "Thermochemical Data for Pure Substances." VCH, Weinheim, New York, 1989.
29. R. Morineau and M. Paulus, *Phys. Status Solidi A* **20,** 373 (1973).